J. Biochem. **129**, 205–208 (2001)

Crystal Structure of *meso*-2,3-Butanediol Dehydrogenase in a Complex with NAD$^+$ and Inhibitor Mercaptoethanol at 1.7 Å Resolution for Understanding of Chiral Substrate Recognition Mechanisms[1]

Masato Otagiri,* Genji Kurisu,* Sadaharu Ui,† Yusuke Takusagawa,† Moriya Ohkuma,‡ Toshiaki Kudo,‡ and Masami Kusunoki*,[2]

**Institute for Protein Research, Osaka University, Suita, Osaka 565-0871; †Department of Applied Chemistry and Biotechnology, Faculty of Engineering, Yamanashi University, Kofu, Yamanashi 400-8511; and ‡The Institute of Physical and Chemical Research (RIKEN), Hirosawa 2-1, Wako, Saitama 351-0198*

Received November 14, 2000; accepted December 18, 2000

The crystal structure of a ternary complex of *meso*-2,3-butanediol dehydrogenase with NAD$^+$ and a competitive inhibitor, mercaptoethanol, has been determined at 1.7 Å resolution by means of molecular replacement and refined to a final *R*-factor of 0.194. The overall structure is similar to those of the other short chain dehydrogenase/reductase enzymes. The NAD$^+$ binding site, and the positions of catalytic residues Ser139, Tyr152, and Lys156 are also conserved. The crystal structure revealed that mercaptoethanol bound specifically to *meso*-2,3-butanediol dehydrogenase. Two residues around the active site, Gln140 and Gly183, forming hydrogen bonds with the inhibitor, are important but not sufficient for distinguishing stereoisomerism of a chiral substrate.

Key words: butanediol dehydrogenase, chiral recognition, crystal structure, *Klebsiella pneumoniae*, short-chain dehydrogenase/reductase family, stereoisomer.

2,3-Butanediol dehydrogenases (BDHs) catalyze the oxidation of 2,3-butanediol (BD) to acetoin (AC) with NAD$^+$ as the coenzyme, and are classified into at least three types according to their stereospecificity as to substrates and products (*1*): D-BDH catalyzes D(−)-BD to D(−)-AC, L-BDH catalyzes L(+)-BD to L(+)-AC, and *meso*-BDH catalyzes *meso*-BD to D(−)-AC. The stereospecificity of the enzymes, however, has not yet been clarified based on their three-dimensional structures. We are interested in the mechanisms of enzymatic recognition of chiral compounds, and hence have characterized *meso*-BDH from *Klebsiella pneumoniae* (*2*) and L-BDH from *Brevibacterium saccharolyticum* (*3*). These BDHs are each a tetrameric enzyme with a molecular weight of approximately 100 kDa (*2*). In previous studies we analyzed their nucleotide sequences and established their expression systems in *Escherichia coli* (*2*, *3*). *meso*-BDH and L-BDH exhibit 50% identity in amino acid sequence and belong to the short chain dehydrogenase/reductase family (SDR family) (*4*). The SDR enzymes, including *meso*-BDH and L-BDH, have an N-terminal coenzyme-binding motif of GXXXGXG and an active site motif of YXXXK. It is likely that the two BDHs share the catalytic mechanisms with the SDR enzymes and recognize different stereoisomers of BD (Fig. 1b) by means of ingenious mechanisms while catalyzing the same dehydrogenation reaction. We report the crystal structure of *meso*-BDH from *K. pneumoniae* in a complex with a substrate analogue, mercaptoethanol, determined at 1.7 Å resolution to elucidate the stereospecific recognition mechanisms.

meso-BDH was produced as a recombinant protein as described previously (*2*). We tried to crystallize *meso*-BDH in a complex with NAD$^+$ and substrate *meso*-BD by the hanging drop vapor diffusion method (*5*). However, only crystals of *meso*-BDH in a complex with mercaptoethanol instead of *meso*-BD were obtained, as described later. Each 10 μl droplet comprised equal volumes of a reservoir solution containing 20% PEG6000, 1% mercaptoethanol, 200 mM magnesium acetate, 1 mg/ml NAD$^+$, and 20% glucose in 50 mM HEPES (pH 7.2), and a solution of 10 mg/ml protein in 20 mM Tris/HCl (pH 8.0), 100 mM *meso*-BD, and 200 mM NaCl. The droplet was equilibrated against the reservoir solution at 293 K. Crystals grew within one week up to a size of 0.2 × 0.2 × 1.0 mm. X-ray data were collected with an R-axisIV++ (Rigaku) image plate detector system with synchrotron radiation of 0.9000 Å wavelength at beamline 40B2, SPring-8, Hyogo. A crystal was flash-cooled in a nitrogen gas stream and its temperature was maintained at 100 K. The crystals belong to monoclinic space group $P2_1$ with cell dimensions of a = 69.16 Å, b = 109.78 Å, c = 127.28 Å, and β = 102.29°. A total of 203,217 reflections was measured up to 1.7 Å resolution with a completeness of 100% and an R_{meas}, an improved version of R_{merge}, of 0.054. The completeness and R_{meas} for the outermost shell (1.79–1.70 Å) were 100% and 0.192, respectively. Assuming eight monomers per asymmetric unit, the V_m value (*6*) was calculated to be 2.2 Å^3 Da^{-1}, this being in the range for common protein crystals. Data were processed with programs DPS/MOSFLM (*7*) and SCALA in the CCP4 package (*8*). The structure was solved by molecu-

[1] This study was partly supported by grants from MESSC (G.K. and M.K.) and ACT-JST (M.K.).

[2] To whom correspondence should be addressed. E-mail: kusunoki@protein.osaka-u.ac.jp

Abbreviations: AC, acetoin; BD, 2,3-butanediol; BDH, butanediol dehydrogenase; MLCR, mouse lung carbonyl reductase; SDR, short-chain dehydrogenase/reductase.

lar replacement with program AMoRe (*9*) in the CCP4 package using the crystal structure of mouse lung carbonyl reductase (MLCR: pdb code 1CYD) (*10*), which exhibits 30% sequence identity with *meso*-BDH, as a search model. Refinement was carried out with program CNS of version 0.9 (*11*). Five percent of the reflections were set aside for R_{free} calculations (*12*). A molecular model was built using program O (*13*), and was improved through many steps by alternate cycles of model building and crystallographic refinement with CNS, where restraints of non-crystallographic symmetry were applied but removed at the later stages. The results of data collection and refinement statistics are shown in Table I. The stereochemistry of the model was checked with program PROCHECK (*14*), as summarized in Table I. The final *R*-factor and R_{free} for all reflections between 40–1.7 Å resolution were 0.194 and 0.210, respectively.

The crystal structure of a ternary complex of *meso*-BDH/NAD$^+$/mercaptoethanol determined here revealed eight subunits per asymmetric unit. The structures of the eight subunits are similar with an averaged pairwise rms deviation of 0.46 Å for 256 Cα atoms. *meso*-BDH is known to exist as homotetramers in solution (*2*), and has an oblate shape with dimensions of about 70 Å × 85 Å × 50 Å with 222 molecular symmetry. The subunit interactions found in *meso*-BDH are essentially the same as those in tetrameric SDR enzymes of known structure, such as 3α,20β-hydroxysteroid dehydrogenase (*15–17*), 7α-hydroxysteroid dehydrogenase (*18*), and MLCR.

The subunit of *meso*-BDH is a single-domain protein with the α/β doubly wound structure (*19*), as shown in Fig. 1a. The core of the domain is a seven-stranded parallel β-sheet (βA-βG) flanked by six parallel α-helices (αB-αG), three on each side of the β-sheet. This supersecondary structure is essentially composed of two βαβαβ units, which together constitute the dinucleotide-binding motif, the Rossmann fold (*20*). In addition, two short α-helices (αFG1 and αFG2) form a small lobe on top of the core structure. The subunit of *meso*-BDH has the same fold as those of the SDR enzymes, and hence *meso*-BDH belongs to the SDR family in terms of both amino acid sequence and three-dimensional structure. The three-dimensional structure of *meso*-BDH was compared with those of three SDR members exhibiting high sequence homology to *meso*-BDH; MLCR, 3α,20β-hydroxysteroid dehydrogenase and Tropinone reductase II (*21*). A least squares fit of Cα atoms of these enzymes to *meso*-BDH gave rms deviations of 2.24 Å, 1.88 Å, and 1.82 Å for 232, 232, and 230 Cα atoms, respec-

TABLE I. **Data collection and refinement statistics for *meso*-BDH.**

Space group	$P\,2_1$
Cell dimensions (Å)	a = 69.16
	b = 109.78
	c = 127.28
	β = 102.29°
Completeness (%), overall/outermost shell	100.0/100.0 [1.79–1.70]
R_{meas}*, overall/outermost shell	0.054/19.2 [1.79–1.70]
Resolution (Å)	40.0–1.7
No. of reflections	203,217
No. of non-hydrogen atoms:	
protein	14904
coenzyme	352
2-mercaptoethanol	32
glucose	96
Mg^{2+}	4
solvent	839
R-factor	0.193
R_{free}	0.209
R.m.s. deviations from ideal values	
bond length (Å)	0.006
bond angles (°)	1.3
dihedral angles (°)	25.2
improper angles (°)	0.70
Ramachandran plot	
most favored (%)	91.9
allowed (%)	8.1

*$R_{meas} = \Sigma_h(n_h/(n_h - 1))^{1/2} \Sigma_i |I_h - I_{h,i}| / \Sigma_h \Sigma_i I_{h,i}$, where n_h, I_h, and $I_{h,i}$ are the multiplicity, intensity, and ith intensity measurement of reflection *h*, respectively. Values in square brackets are the resolution ranges in Å for the outermost shell.

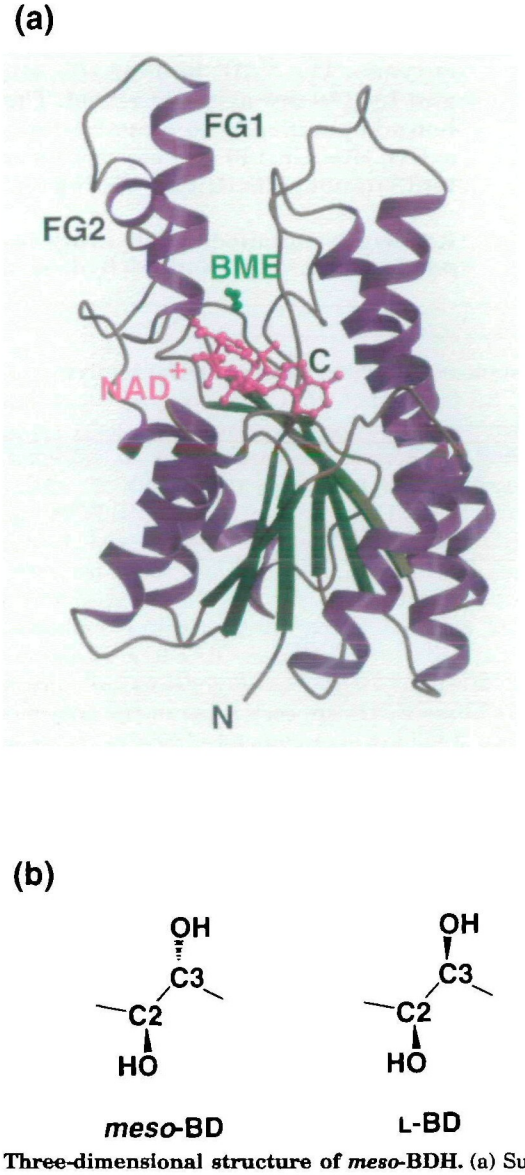

Fig. 1. **Three-dimensional structure of *meso*-BDH.** (a) Subunit structure of *meso*-BDH. NAD$^+$ is colored in magenta, mercaptoethanol (BME) in green, α-helices in purple, and β-strands in dark-green. NAD$^+$ and mercaptoethanol are shown as ball-and-stick models. The N- and C-termini, and α-helices FG1 and FG2 are also indicated. (a) was drawn with program BOBSCRIPT (*23*) and Raster 3D (*24*). (b) Structure of *meso*-BD and L-BD.

tively, indicating a high level of structural similarity. Major structural differences were found at residues 190 to 217 of *meso*-BDH, the segment including short α-helices αFG1 and αFG2. The bound NAD^+ molecules are in an extended conformation with the adenine ring in the *anti* conformation and the nicotinamide ring in the *syn* conformation, this being quite similar to in the cases of most SDR members. Both the ribose rings have $^2E(C2'\text{-}endo)$ puckering. The *syn* conformation of the nicotinamide ring allows *meso*-BDH to transfer the *pro*-S hydride ion (B-face) to a substrate.

The SDR enzymes have a highly conserved Ser-Tyr-Lys triad at the active site, and their catalytic roles have been intensively studied (*10*, *21*, *22*). The conserved Tyr residue acts as an acid-base catalyst for proton transfer, while the Lys residue is important in cofactor binding and in lowering the pK_a value of the Tyr. The serine residue is suggested to be involved in the binding of a substrate. Amino acid sequence alignment of *meso*-BDH with SDRs revealed Ser139, Tyr152, and Lys156 are the triad. These three catalytic residues are located in the active site cleft and their spatial arrangements are common to those of the other SDR enzymes (Fig. 2a). These results indicate that *meso*-BDH catalyzes the dehydrogenation reaction through a similar mechanism for the other SDR enzymes using the Ser-Tyr-Lys catalytic triad.

During refinement, difference Fourie maps showed electron density located in the cleft of *meso*-BDH. We attributed this to the substrate or product, but could not build a model of BD or AC suitably into the electron density map, which was, however, clear enough and had a resolution of 1.7 Å. Then the electron density was suspected to be due to a molecule of mercaptoethanol, which was added in a large quantity to the crystallization solution. Assignment of the electron density to a mercaptoethanol molecule led to a better fit of electron density and refinement producing an omit-map indicative of a high electron density portion suitably attributable to the S atom of mercaptoethanol (Fig. 2a). A crystal without mercaptoethanol was prepared but gave X-ray diffraction of lower resolution, thus providing no significant information. We confirmed that mercaptoethanol inhibits *meso*-BDH competitively (K_i = 0.517 mM at pH 8.0), and hence concluded that the electron density to be due to a mercaptoethanol molecule. Figure 2b shows a model for mercaptoethanol and NAD^+ together with active site residues of *meso*-BDH. We present here a working hypothesis for the mode of binding of *meso*-BD based on the binding of mercaptoethanol (Fig. 2c). The C2 and C3 carbon atoms of *meso*-BD, the real substrate, are in the *S* and *R*

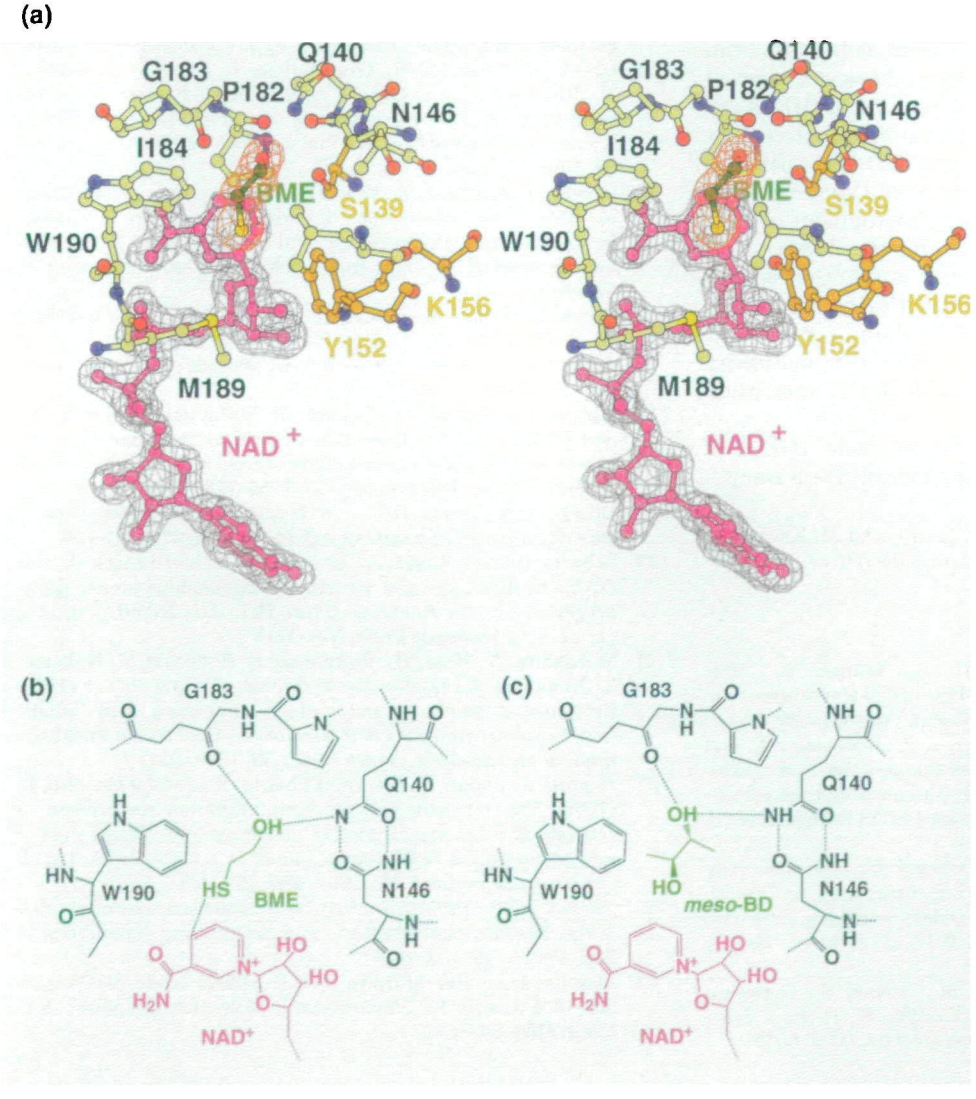

Fig. 2. **Diagrams of the active site.** (a) Ball-and-stick models for NAD^+, mercaptoethanol (BME), and protein residues around the catalytic site, where a (2*Fo* – *Fc*) map at 1.7 Å is superimposed on NAD^+ and mercaptoethanol at the 1.0 σ level. The inhibitor, mercaptoethanol, is colored in green, NAD^+ in magenta, and the catalytic triad in orange. Carbon, oxygen, nitrogen, and sulfur atoms are colored in cream, red, blue, and yellow for protein residues and mercaptoethanol [only (a)]. (a) was generated with program BOBSCRIPT. (b) Model for mercaptoethanol, a competitive inhibitor, based on the results of crystal analysis. (c) Proposed model for *meso*-BD, the real substrate.

configurations, whereas those of L-BD, a stereoisomer of the substrate, are both in the *S* configuration (Fig. 1b). The only difference between *meso*-BD and L-BD is the configuration at C3. Some protein residues of *meso*-BDH most likely interact with the C3 hydroxyl group of *meso*-BD to distinguish the configuration at C3. As shown in Fig. 2b, the carbonyl group of Gly183 and the side chain NH of Gln140 form hydrogen bonds with the C3 hydroxyl group of the mercaptoethanol. Mercaptoethanol, a competitive inhibitor, should mimic the binding mode of substrate *meso*-BD and thus it may be assumed that the hydroxyl group of the mercaptoethanol occupies the position of the C3 hydroxyl group of BD. Sequence comparison between *meso*-BDH and L-BDH showed that only Gln140 and Asn146 of *meso*-BDH differ from L-BDH among the residues surrounding the mercaptoethanol. These two residues may be responsible for the recognition of *meso*-BD as opposed to L-BD. In order to verify this hypothesis, a mutant enzyme with Gln140 replaced by Ile mimicking Ile142 of L-BDH was prepared and its activity was measured. The Gln140Ile mutant exhibited no activity with *meso*-BD or L-BD, indicating that the proposed mode of binding of *meso*-BD based on the mercaptoethanol binding is effective in this respect and that Gln140 plays an important role in chiral substrate recognition. We prepared a double mutant enzyme in which Gln140 and Asn146 were changed to Ile and Phe, *i.e.* corresponding to the residues of L-BDH, respectively, to convert the enzyme's streospecificity for a chiral substrate from *meso*-BD to L-BD. The double mutant, however, showed only a low level of activity with L-BD and *meso*-BD, as opposed to our design. This indicates that simple replacement of the two residues that differ in *meso*-BDH and L-BDH is not sufficient for conversion of the substrate stereospecificity, and that subtle differences in the environment around the catalytic cleft may be responsible for the difference in substrate stereospecificity. We are now attempting crystal structure determination of L-BDH to clarify the subtle structural differences between *meso*-BDH and L-BDH with the expectation of converting the substrate stereospecificity and of deepening our understanding of chiral recognition by BDHs.

The coordinates and structure factors (code 1GEG) of *meso*-BDH have been deposited in the Protein Data Bank.

We wish to thank Drs H. Moriyama, K. Miura, and M. Kawamoto of JASRI for the assistance during the data collection at SPring-8.

REFERENCES

1. Ui, S., Matsuyama, N., Masuda, H., and Muraki, H. (1984) Mechanism for the formation of 2,3-butanediol stereoisomers in *Klebsiella pneumoniae*. *J. Ferment. Technol.* **62**, 551–559
2. Ui, S., Okajima, Y., Mimura, A., Kanai, H., Kobayashi, T., and Kudo, T. (1997) Sequence analysis of the gene for and characterization of D-acetoin forming *meso*-2,3-butanediol dehydrogenase of *Klebsiella pneumoniae* expressed in *Escherichia coli*. *J. Ferment. Bioeng.* **86**, 290–295
3. Ui, S., Otagiri, M., Mimura, A., Dohmae, N., Takio, K., Ohkuma, M., and Kudo, T. (1998) Cloing, expression and nucleotide sequence of the L-2,3-butanediol dehydrogenase gene from *Brevibacterium saccharolyticum* C-1012. *J. Ferment. Bioeng.* **83**, 32–37
4. Jörnvall, H., Persson, B., Krook, M., Atrian, S., Gonzalez-Duarte, R., Jeffery, J., and Ghosh, D. (1995) Short-chain dehydrogenases/reductases (SDR). *Biochemistry* **34**, 6003–6013
5. McPherson, A. (1982) *Preparation and Analysis of Protein Crystals*, 1st ed., pp. 96–97, John Wiley, New York
6. Matthews, B.W. (1968) Solvent content of protein crystals. *J. Mol. Biol.* **33**, 491–497
7. Rossmann, M.G. and van Beek, C.G. (1999) Data processing. *Acta Crystallogr. D Biol. Crystallogr.* **55**, 1631–1640
8. Collaborative Computational Project, Number 4 (1994) The CCP4 suite: programs for protein crystallography. *Acta Cryst.* **D50**, 760–763
9. Navaza, J. (1994) AMoRe: an atomated package for molecular replacement. *Acta Crystallogr. Sect. A* **50**, 157–163
10. Tanaka, N., Nonaka, T., Nakanishi, M., Deyashiki, Y., Hara, A., and Mitsui, Y. (1996) Crystal structure of the ternary complex of mouse lung carbonyl reductase at 1.8 Å resolution: the structural origin of coenzyme specificity in the short-chain dehydrogenase/reductase family. *Structure* **4**, 33–45
11. Brünger, A.T., Adams, P.D., Clore, G.M., DeLano, W.L., Gros, P., Grosse-Kunstleve, R.W., Jiang, J.S., Kuszewski, J., Nilges, M., Pannu, N.S., Read, R.J., Rice, L.M., Simonson, T., and Warren, G.L. (1998) Crystallography and NMR system: A new software suite for macromolecular structure determination. *Acta Crystallogr. D Biol. Crystallogr.* **54**, 905–921
12. Brünger, A.T. (1992) Free *R* value: a novel statistical quantity for assessing the accuracy of crystal structures. *Nature* **355**, 472–474
13. Jones, T.A., Zou, J.Y., Cowan, S.W., and Kjeldgaard, M. (1991) Improved methods for binding protein models in electron density maps and the location of errors in these models. *Acta Crystallogr. A* **47**, 110–119
14. Laskowski, R.A., MacArthur, M.W., Moss, D.S., and Thornton, J.M. (1993) PROCHECK: a program to check the stereochemical quality of protein structures. *J. Appl. Crystallog.* **5**, 802–810
15. Ghosh, D., Weeks, C.M., Grouchulski, P., Duax, W.L., Erman, M., Rimsay, R.L., and Orr, J.C. (1991) Three-dimensional structure of holo 3α,20β-hydroxysteroid dehydrogenase: a member of a short-chain dehydrogenase family. *Proc. Natl. Acad. Sci. USA* **88**, 10064–10068
16. Ghosh, D., Wawrzak, Z., Weeks, C.M., Duax, W.L., and Erman, M. (1994) The refined three-dimensional structure of 3α,20β-hydroxysteroid dehydrogenase and possible roles of the residues conserved in short-chain dehydrogenases. *Structure* **2**, 629–640
17. Ghosh, D., Erman, M., Wawrzak, Z., Duax, W.L., and Pangborn, W. (1994) Mechanism of inhibition of 3α,20β-hydroxysteroid dehydrogenase by a licorice-derived steroidal inhibitor. *Structure* **2**, 973–980
18. Tanaka, N., Nonaka, T., Tanabe, T., Yoshimoto, T., Tsuru, D., and Mitsui, Y. (1996) Crystal structures of the binary and ternary complexes of 7 alpha-hydroxysteroid dehydrogenase from *Escherichia coli*. *Biochemistry* **35**, 7715–7730
19. Orengo, C.A., Jones, D.T., and Thornton, J.M. (1994) Protein superfamilies and domain superfolds. *Nature* **372**, 631–634
20. Rossmann, M.G., Liljas, A., Branden, C.-I., and Banaszak, L.J. (1975) Evolutionary and structural relationships among dehydrogenases in *The Enzymes* (Boyer, P.D., ed.), 3rd ed., Vol. 11A, pp. 61–102, Academic Press, New York
21. Yamashita, A., Kato, H., Wakatsuki, S., Tomizaki, T., Nakatsu, T., Nakajima, K., Hashimoto, T., Yamada, Y., and Oda, J. (1999) Structure of tropinone reductase-II complexed with $NADP^+$ and pseudotropine at 1.9 Å resolution: implication substrate binding and catalysis. *Biochemistry* **38**, 7630–7637
22. Benach, J., Atrian, S., Gonzàlez-Duarte, R., and Ladenstein, R. (1999) The catalytic reaction and inhibition mechanism of *Drosophila lebanonensis* alcohol dehydrogenase: observation of an enzyme-bound NAD-ketone adduct at 1.4 Å resolution by X-ray crystallography. *J. Mol. Biol.* **289**, 335–355
23. Esnouf, R.M. (1997) An extensively modified version of MolScript that includes greatly enhanced coloring capabilities. J. *Mol. Graph.* **15**, 133–138
24. Merritt, E.A. and Murphy, M.E.P. (1994) Raster3D Version 2.0—A Program for Photorealistic Molecular Graphics'. *Acta Cryst.* **D50**, 869–873